RSC Advances

ROYAL SOCIETY OF CHEMISTRY

www.rsc.org/advances

Journal Name

ARTICLE

Nanomorphology-dependent pseudocapacitive properties of NiO electrodes engineered through controlled potentiodynamic electrodeposition process†

Received 00th January 20xx,
Accepted 00th January 20xx

DOI: 10.1039/x0xx00000x
www.rsc.org/

Rohan M. Kore,[a] Rajaram S. Mane,[b,c] Mu. Naushad,[c] Mohammad R. Khan,[c] and Balkrishna J. Lokhande[a,*]

Three nickel oxide (NiO) electrdes of diferent morphologies have been successfully engineered through a controlled potentiodynamic electrodeposition process in the presence of different nickel precursors. Effect of nickel precursors on structural, morphological and pseudocapacitive properties of NiO thin film electrodes have been systematically investigated. The stucural information obtained from the X-ray diffraction patterns confirms the formation of cubic structured NiO. The field-emission scanning electron microscopic images endorses for the evolution of uniformly distributed up-grown nanoflakes, irregular nanoflake-like and a well-covered porous architecture comprised of interconnected uniform nanoflakes of NiO nanostructures with surface contact angle values 126°, 148° and 104°. The effect of the developed NiO nanostructures on pseudocapacitance behavior has been thoroughly investigated using cyclic voltammetry, chronopotentiometric charge-discharge and electrochemical impedance spectroscopy measurement techniques. The optimal specific capacitance of 893 Fg^{-1} has been achieved for NiO electrode having interconnected nanoflake-type morphology at the scan rate of 5 mVs^{-1}. Furthermore, these NiO electrodes have demonstrated long-term cycling stability in KOH electrolyte. The electrochemical impedance spectroscopy measurements carried out on developed NiO nanostructured electrodes corroborate that, NiO electrode composed of uniformly distributed interconnected nanoflakes is best and suitable electrode for good capacity electrochemical supercapacitor among others.

Introduction

The development of human civilization and advancement of modern technology have made energy at the centre of everlasting quest. An important intermediate step towards versatile and efficient energy applications includes energy storage and its transportation with minimum losses. Most effective and practical technologies, presently preferred, for electrochemical energy storage comprises batteries, fuel cells and electrochemical supercapacitors (ECs). ECs or ultracapacitors have attracted significant attention, mainly due to their high power density, long lifecycle and bridging function for the power/ energy gap between traditional capacitors (high power output) and batteries/fuel cells (high energy storage).[1-3] However, depending on the charge storage mechanism as well as active materials used, ECs are classified into two categories. One, in electrochemical double layer capacitors (EDLCs), where carbon-based active materials, graphene etc., are in general considered, which stores charges at electrode/electrolyte interface. While in second type i.e. pseudocapacitors or redox supercapacitors, charge storage in electrode materials like transition metal oxides as well as electrically conducting polymers takes place through fast and reversible surface/near-surface reactions.[4] Among various transition-metal oxides including RuO_2, IrO_2, MnO_2, NiO, Co_2O_3, SnO_2, Fe_2O_3, V_2O_5 etc.,[5-13] nickel oxide (NiO) has found considerable attention and interest, due to its high theoretical capacity (2573 F g^{-1}), low-cost, low-toxicity, low environmental impact and sufficiently large pseudo-capacitive behaviour.[14,15] There are several methods so far used to tune the size, shape and morphology of electrode used for EC. Commonly, layered nickel hydroxide ($Ni(OH)_2$) with various morphologies can be synthesized from solution methods like chemical precipitation,[16] electrodeposition,[17] followed by thermal decomposition using solutions of Ni(II). Lee *et al.* synthesized hierarchical microspheres of α- $Ni(OH)_2$ nanosheets, intercalated with desired anionic species (Cl^-, NO_3^-, OAc^-, and SO_4^{2-}), and showed change in specific capacitance as a function of size of the intercalated anion.[18] Dubal *et al.* developed different nanostructures of β-$Ni(OH)_2$ using chemical bath deposition method from different nickel precursors.[19] It is inferred that, the surface morphology and

[a] *Supercapacitive Studies Laboratory, School of Physical Sciences, Solapur University, Solapur. 413255 (M. S.), India. Email: bjlokhande@yahoo.com, rmkore@sus.ac.in*
[b] *Centre for Nanomaterials & Energy Devices, School of Physical Sciences, SRTM, University, 431606, Nanded, India.*
[c] *Department of Chemistry, College of Science, Bld#5, King Saud University, Riyadh, Saudi Arabia.*
**Address to whom all correspondence can be addressed.*
†Electronic Supplementary Information (ESI) available: Figure S1-S3 and Electronic circuitry parameters Table S1. DOI: 10.1039/x0xx00000x

the porosity of NiO are strongly influenced by the use of anions salt during hydrothermal synthesis process which eventually also affects on the pseudocapacitance and the power density performances.[20]

This work emphasizes on the effect of precursors containing different anions like NO_3^-, Cl^- and SO_4^{2-} on physical properties and pseudo-capacitive performances of NiO thin film electrodes obtained by a controlled potentiodynamic electrodeposition process. The different morphologies of NiO electrodes corroborate different charge transport kinetics on account of presence of various pathways.

Experimental details

All the chemicals used during experiment were of analytical grade reagent, purchased from Thomas Baker (Chemicals) PVT. LTD. and were used without any further purification. Double-stilled water prepared in laboratory was used as the solvent. Template- and binder-free electroplated Ni thin film electrodes were prepared from different anionic precursors like $NiCl_2.6H_2O$, Ni $(NO_3)_2.6H_2O$, Ni $SO_4.6H_2O$ at room temperature using a three electrode set up. Stainless-steel (SS, Sr. No. 304) pieces of 1 X 5 cm^2 dimensions were used for developing NiO electrodes of different morphologies. Prior to deposition, SS pieces were well-polished by using a 320 grade silicon carbide paper to a rough finish and further cleaned with acetone followed by ultrasonic cleaning. The graphite plate (2 x 5 cm^2) and saturated calomel electrode (SCE) were used as the counter and the reference electrodes, respectively. The plating bath contained aqueous Ni salt of 0.1 M during each experiment. Potentiodynamic electrodeposition process was carried out by using CHI 408C electrochemical analyser workstation (CH Instruments USA). The deposition was performed within the potential windows of -0.75 — -0.6 V, -0.7 — -0.55 V and -0.8 — -0.65 V for chloride, nitrate and sulphate salts, respectively (i.e. 0.15 V CV window for each) at the scan rate of 100 mV/s for 30 min each [Figure S1 (a-c) of Supporting Information]. After deposition, electroplated Ni electrodes were washed with distilled water and dried at room temperature. Furthermore, for converting to NiO, these electrodes were air-annealed at 500 ℃ for 2 h. Electrodes so obtained from nitrate, chloride and sulphate precursors were symbolized as NiO-N, NiO-C and NiO-S, respectively. The active mass of the deposited NiO in every case was estimated using sensitive gravimetric weight difference method (Analytical single pan microbalance, TAPSON-Model 100-TS). The masses on above three NiO electrodes were respectively 0.04, 0.03 and 0.05 mg.

For the structural elucidation and morphological evolution confirmation, X-ray diffraction (XRD) patterns (Rigaku D/ max 2550 Vb+18 kW X-ray diffractometer with Cu Kα radiation (λ= 0.15405 nm)) and field-emission scanning electron microscopy (FESEM; MIRA3, TESCAN) digital photoimages, respectively, were considered. Contact angle measurements were carried out using Holmark Contact Angle Meter (Model No. HO-IAD-CAM-01B) equipment with a charge-coupled device. Electrochemical performances were evaluated by cyclic voltammetry (CV), chronopotentiometry (CP) and electrochemical impedance spectroscopy (EIS) measurement techniques with three electrode cell configuration consisting of platinum wire and SCE as counter electrode and reference electrodes, respectively, in 1 M KOH electrolyte.

Results and discussion

CV method was exploited for the controlled potentiodynamic electrodeposition process. The reduction of Ni^{+2} species was observed during potential range of -0.6 — -0.8 V as reported by Jagadale *et al.*[21] The potential window was restricted at -0.75, -0.7 and -0.8 V for chloride, nitrate and sulphate salts, respectively to obtain the Ni plated film electrodes. The process can be represented by the following reaction;

$$NiCl_2.6H_2O \xrightarrow{-0.75\ V\ to -0.6\ V} Ni^{+2} + 2Cl^-$$

$$Ni(NO_3)_2\,6H_2O \xrightarrow{-0.7\ \text{V to}\ -0.55\ \text{V}} Ni^{+2} + 2NO_3^-$$

$$NiSO_4.6H_2O \xrightarrow{-0.8\ \text{V to}\ -0.65\ \text{V}} Ni^{+2} + SO_4^{2-}$$

Here Ni^{+2} species condense on the SS to form electroplated Ni thin film electrodes which were later heat treated at 500℃ for 2 h to obtain NiO.[22]

Figure 1 presents the XRD spectra of NiO-N, NiO-C and NiO-S electrodes. Presence of the broad diffraction peaks of various intensities supported for the nanocrystallinity of the obtained products. The observed diffraction peaks confirms the cubic phase of NiO. Peaks at 37.2°, 43.2° and 62.8°, belongs to (111), (200) and (220) crystallographic planes, were consistent to planes found in JCPDS 78-0429 file for cubic NiO. Peaks marked by asterisk were assigned to used substrate i.e. SS.

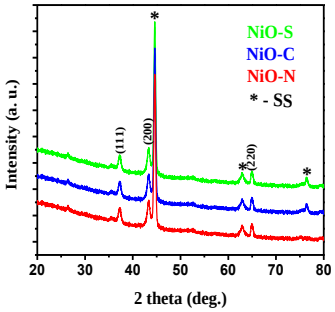

Figure 1 XRD patterns of NiO electrodes prepared using nitrate, chloride and sulphate precursors on SS substrate.

Figure 2 depicts the schematic representation of the plausible reaction mechanism and steps involved during the formation of NiO nanostructures. Nucleation and initial growth to form Ni-electroplated film and the final growth for individual morphology evolution has been clearly demonstrated. During

the electroplating of nickel metal ions, the nucleation and the initial growth was influenced by the anions like NO_3^-, Cl^- and

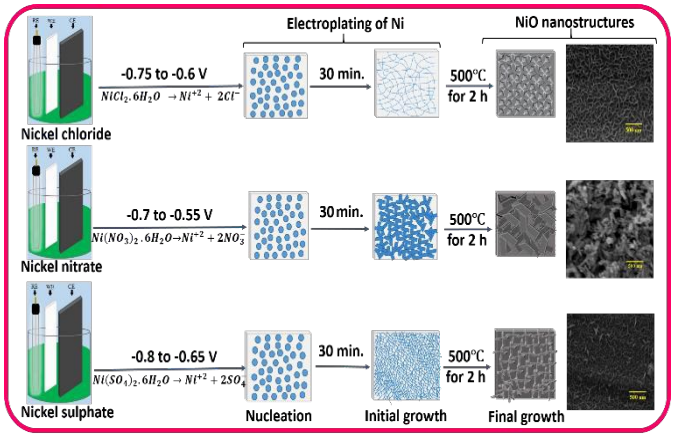

Figure 2 Schematic representations for developing different nanostructures of NiO.

SO_4^{2-} due to their different over-potentials. The over-potential for different anions of the precursors used in the present investigation changes in the order $Cl^- < NO_3^- < SO_4^{2-}$. The higher overpotential of SO_4^{2-} anions enabled initial growth of uniformly distributed interconnected nano-flakes. Comparatively lower over-potential of Cl^- anions had potential to form small number of initial nuclei, onto which further adsorption of Ni^{+2} ions might be occurred to form up grown nano-flakes. Whereas, moderate over potential of NO_3^- anions could result in the formation of randomly distributed flake-like architecture.[23, 24]

Figure 3 (a-b, c-d and e-f) represents the plane-view FESEM images of NiO-C, NiO-N and NiO-S thin film electrodes at low and high magnification. Complete substrate surface was covered with uniformly distributed up-grown nanoflakes [Fig. 3(a, b)] for the NiO-C electrode, consistent to previous result wherein synthesis of various $Ni(OH)_2$ thin film electrodes was carried out using chemical bath deposition method.[19] Figure 3(c, d) shows FESEM micrographs of NiO-N electrodes, which contains irregular nanoflake-type architecture with few air voids. Analogous result for NiO was reported by Vijayakumar *et al.*[8] by using microwave-assisted method [Fig. 3(d)]. Figure 3(e, f) shows that the NiO-S electrode surface was made-up of well covered, porous, interconnected nanoflake-type nanostructure. Similar type of NiO nanostructure was reported by Chen *et al.*[25] prepared using a hydrothermal method. Figure S2 (a, b, c) represents cross-sectional SEM images of NiO- C, NiO- N and NiO-S electrodes. The observed thicknesses for NiO-C, NiO-N and NiO- S were 18, 21 and 33 (±2) µm, respectively.

The interfacial tensions, between the water/air, water/solid, and solid / air interfaces, decide the wettability of solid with water and the ratio between these tensions fixes the contact angle (θ) between water droplet with the surface, in contact. In fact, it has considerable influence on the EC performance. The

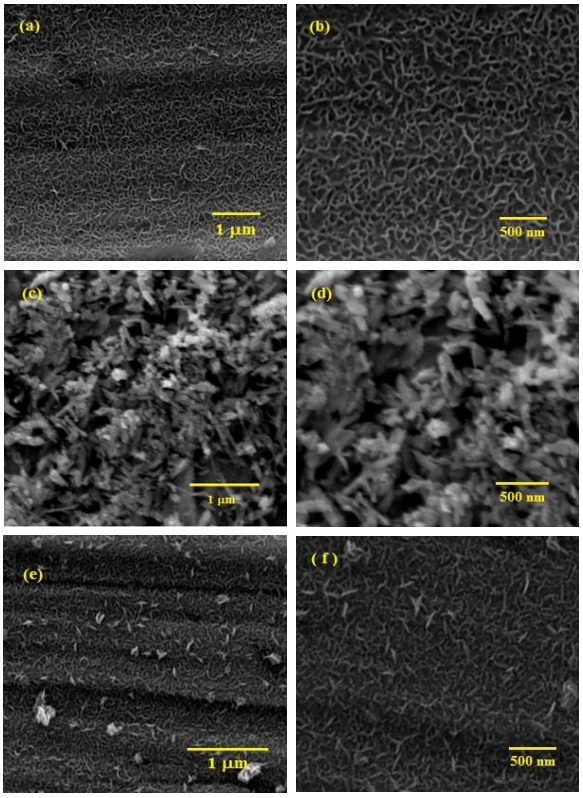

Figure 3 FESEM plan-views of; (a, b) NiO-C, (c, d) NiO- N, and (e, f) NiO-S electrodes.

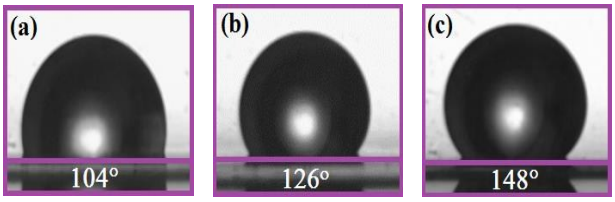

Figure 4 Contact angle measurements on; (a) NiO-S (b) NiO-C, and (c) NiO-N electrode surfaces.

surface wettability involves the interaction between the liquid and the solid in contact. The contact angle measurement provides information about surface wettability. In general, surface water contact angle is inversely proportional to the wettability, fixed from the Young's relation. [26] Alternatively, the contact angle value depends upon local inhomogeneity, chemical composition and the surface morphology of the electrode. The contact angle values obtained on NiO-S, NiO-C and NiO-N electrode surfaces were 104°, 126° and 148°, respectively [Figure 4 (a-c)]. In recent work of Vadiyar *et al.*,[27] it is reported that for higher specific capacitance contact angle value should be less than 20° thereby, there is need to alter surface architecture/functional group so that obtained contact angle value will be lowered, which is ongoing work.

The CV spectra of NiO-N, NiO-C and NiO-S electrodes performed at a scan rate of 5 mV/s within a potential range of 0—0.45 V (*vs.*

SCE) in 1 M KOH electrolyte are presented in Fig. 5 (a). The electrochemical parameters derived from the CV curves are summarized in Table-1. Before measurements, all electrodes were stabilized for 20 CV cycles. All the electrodes shows nearly similar shape with peaks at the respective anodic and cathodic sweeps revealing the pseudocapacitive behaviour, characteristic of a redox mechanism.[28] The peaks, during anodic sweep at positive current density and cathodic sweep at negative current density, occur due to oxidation of Ni^{+2}–Ni^{+3} (charging) and reduction of Ni^{+3}–Ni^{+2} (discharging) processes, respectively. Redox process responsible for these actions can be presented as.[20]

$$NiO + z\ OH^- \rightleftharpoons z\ NiOOH + (1-z)\ NiO + z\ e^- \quad (1)$$

The absence of symmetry, in cathodic sweeps to their corresponding anodic sweeps of CV curves, is attributed to irreversibility in the redox process.[29] Generally, pseudocapacitors involve Faradic redox reactions wherein the ideal reversibility cannot be realized kinetically for the positive and negative sweeps. Also ohmic resistance, caused by electrolyte diffusion during charge intercalation-deintercallation process at the electrodes, contributes to the kinetic irreversibility of the redox reaction.[30, 31] The over-potential ($\Delta E_{O,R}$) also gives an idea about the reversibility in the redox reaction, where smaller value resembles to better reversibility and *vice-versa.* Among the three electrodes, NiO-N showed highest reversibility ($\Delta E_{O,R}$ = 83mV) while NiO-S confirmed the least reversibility ($\Delta E_{O,R}$ = 125mV). Compared with the NiO-C and NiO-N electrodes, the NiO-S electrode demonstrated maximum area under curve. Thereby, NiO-S electrode exhibited better electrochemical properties than others. The results of CV curves were quantified by calculating the specific capacitance (C_S, Fg^{-1}) values using the formula with *v*: potential scan rate ($mV.s^{-1}$), V_c–V_a: potential window, *I*: the response current (mA), and *m*: deposited mass of the active material on each electrode for unit area (1 cm^2) dipped in electrolyte,

$$C_S = \frac{1}{mv(V_c - V_a)} \int_{V_a}^{V_c} I\, dV \quad (2)$$

The NiO-S electrode offered the highest current density and capacitance value whereas NiO-N electrode permitted lowest once. The C_s values depicted from CV curves at the scan rate of 5 mVs^{-1} for NiO-N, NiO-C and NiO-S electrodes were 136, 267 and 893 $F.g^{-1}$ respectively. Fig. 5 (b) shows the C_s values of electrodes for 5, 10, 50, 100 and 150 mVs^{-1} scan rates, wherein, the C_s values were decreased with increase of the scan rate. At higher scan rate, the accessibility of ions entering into all the pores within the electrode materials, and thus the transport of ions was limited due to their slow diffusion. Hence only the outer surface could be utilized for the charge storage.[32] At all scan rates, NiO-S electrode demonstrated high C_s values by providing a larger electro-active surface area for redox reactions and charge storage values compared to NiO-C and NiO-N electrodes. The trend was consistent with surface morphology and contact angle (wettability) measurements. The compact up-grown nanoflake and nanoflake-type nanostructures might not facilitate the electron transport, while the porous architecture comprised of interpenetrating structures could provide a high surface area by enabling active-site accessibility. This might allow effective electron transport during the redox process, responsible for the high specific capacitance. Also the lower contact angle (larger wettability) value of NiO-S electrode than NiO-C and NiO-N electrodes facilitated more surface to be in contact with the electrolyte for better OH^- propagation for maximum faradic reactions.[28]

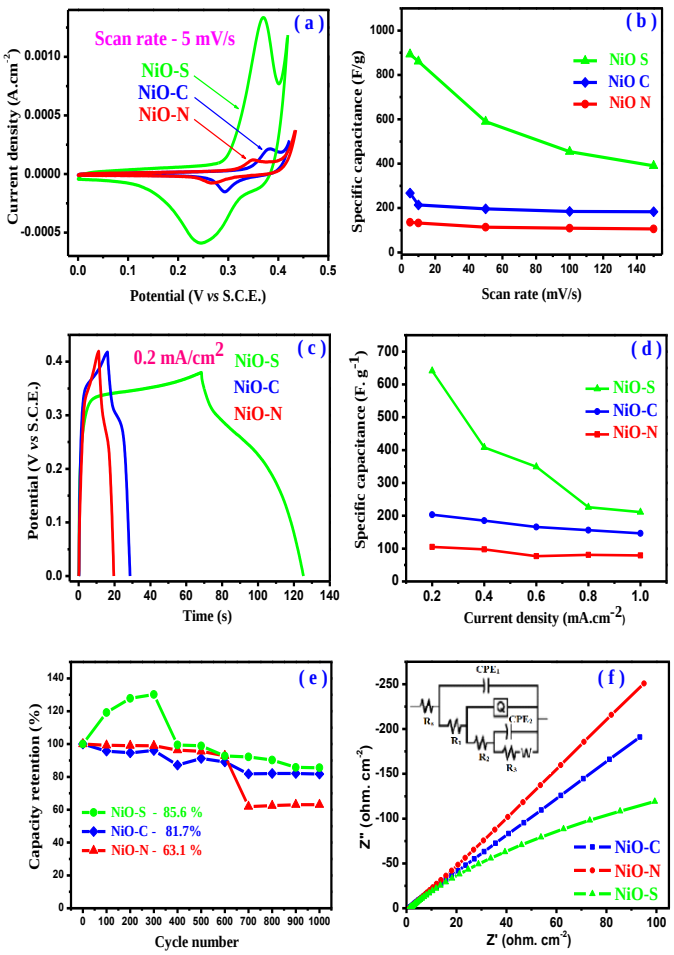

Figure 5 Electrochemical characterizations; (a) cyclic voltammograms, (b) specific capacitance as a function of scan rate, (c) charge discharge measurement curves, (d) specific capacitance as a function of current density, (e) capacitive retention (in %) as a function of cycle number, (f) electrochemical impedance spectroscopic measurements of NiO electrodes (inset shows an equivalent circuit used for modulation), of NiO-N, NiO-C, NiO-S electrodes.

Table 1: Electrochemical parameters from CVs for different NiO samples*

Electrodes	E_O (mV)	E_R (mV)	$\Delta E_{O,R} = E_O - E_R$ (mV)
NiO-S	245	370	125
NiO-C	293	384	91
NiO-N	266	349	83

*E_O and E_R are defined as the oxidation (anodic peak) potential and reduction (cathodic peak) potential respectively.

The electrochemical utilization factors (Z in eqn. (1)) for NiO electrodes were calculated from the following expression,

$$z = \frac{C_S M \Delta V}{F} \quad (3)$$

with a potential window (ΔV) of 0.45 V, molecular weight (M) of 74.692 g for NiO, the Faraday constant of 96487 C/equiv. The C_S values at 5 mV/s scan rate for different NiO electrodes were calculated. A value of z =1 indicates that the entire electroactive material is involved in the redox reaction process. The values of Z for the NiO-N, NiO-C and NiO-S electrodes were 0.043, 0.074 and 0.331, respectively. So the probable active sites involved in the redox reaction for the electrodes, NiO-N, NiO-C and NiO-S were 4.3%, 7.4% and 33.1%, respectively.

Furthermore, CP charge/discharge measurements were carried for all samples in 1M KOH electrolyte at a current density of 0.2 mA.cm^{-2} [Fig. 5 (c)]. The nonlinearity in all electrodes is supporting the pseudocapacitive behaviour, as EDLCs preferably presents a triangular-wave-like profile for a charge/discharge cycle.[33] For comparison with the CV results, the C_S values were also calculated from the charge/ discharge measurement curves. The C_S values obtained for NiO-N, NiO-C and NiO-S electrodes were 105, 203 and 642 F/g, respectively. Furthermore, the Fig. 5 (d) reflects the variation of C_S values with respect to different current densities, like 0.2, 0.4, 0.6, 0.8 and 1 mA.cm^{-2}. The small variation in the C_S values was observed for all the electrodes calculated from CV and charge-discharge measurements curves. This divergence in the results could be due to fact that the C_S values calculated from CV curves was at the particular potential, while that calculated from charge-discharge measurements covered the average capacitance over the potential range 0—0.4 V. This averaging leads to the variation in the C_S value.[34,35]

The large cycling stability of the electrode is the key parameter used for determining characteristics of a supercapacitor, hence the electrochemical stabilities of NiO-N, NiO-C and NiO-S electrodes were evaluated by CV at a scan rate of 100 mV.s^{-1} for 1000 cycles and the plots of capacitive retention with the cycle number are presented in Fig. 5 (e). The % capacity retention values for the NiO-S, NiO-C and NiO-N electrodes were 85.6 %, 81.7% and 63.1%, respectively. The increase in the capacity of the NiO-S electrode for first few hundred cycles was due to the activation of NiO electrode.[36, 37] The maximum retention in capacity of NiO-N electrode was assigned to nanoflake-like morphology which might undergo degradation due to continuous intercalation/de-intercalation of the OH^-.

To inspect the charge transport kinetics and suitability of NiO nanostructured electrodes, the EIS measurement was confined to a frequency range of 0.1 to 10^5 Hz with a potential amplitude of 5 mV/SCE at -0.06453, -0.00668, 0.23872 V potential for NiO-N, NiO-C, NiO-S electrodes, respectively, in 1M KOH solution. Typical Nyquist plots for different NiO electrodes and equivalent circuit are shown in Fig. 5 (f). The equivalent circuit matching was operated by using the ZSimpWin software. The measured and simulated data for matched equivalent circuit is given in Fig S2 (a-c) for all the electrodes and the corresponding equivalent circuit parameters obtained, from simulation, are given in Table S1. The equivalent series resistance of a supercapacitor involves electronic and ionic contributions. The electronic resistance is related to the intrinsic electronic resistance of the NiO particles and the interfacial resistances of particles-to-particles and particles-to-current collector. The ionic resistance is associated with the electrolyte resistance in the pores and the ionic (diffusion) resistance of ions moving in small pores. [38, 39] The equivalent series resistance (ESR) of an electrode was obtained from the intercept of real impedance at high frequency side. The ESR values of NiO-N, NiO-C and NiO-S electrodes were 1.34, 1.29 and 1.27 Ω/cm^2, respectively. From the EIS spectra, electrochemical active surface area used for individual electrode was estimated using the relation reported elsewhere.[40, 41] The obtained surface areas for NiO-N, NiO-C and NiO-S electrodes were 9.67, 17.95 and 91.5 m^{2}g^{-1}, respectively. These results emphasized that the porous architecture with interconnected nanoflake-type morphology and larger surface area of NiO-S electrode could provide a very low impedance and consequently easy access to ions for intercalation/de-intercalation process. This study exposed that lower electronic and ionic resistance of porous architecture with interconnected nanoflakes demonstrated the enhanced capacitive performance of NiO-S electrodes compared to others.

Conclusions

By using a controlled potentiodynamic electrodeposition process, three different nanostructures of NiO were efficaciously engineered using three different nickel salts. Field-emission scanning electron micrograph images revealed the formation of up-grown nanoflakes, irregular nanoflake-like and porous architecture with interconnected nanoflakes of NiO under different synthesis conditions. Contact angle measurement confirmed that the wettability of NiO electrode can be changed with nanostructure type and there is need to modify surface so that water contact angle value will be lower than 20°. Electrochemical performance evaluation demonstrated a noticeable effect of different nanostrucures on pseudocapacitance properties of NiO electrodes with a high specific capacitance of 893 F.gm^{-1}, a low value of electrochemical impedance 1.27 Ω.cm^{-2} and larger surface area of 91.5 m^{2}g^{-1}, for porous architecture comprised of interconnected nanoflakes i.e. NiO-S, suggesting its potential application as supercapacitor electrode material. The above mentioned controlled potentiodynamic electrodeposition process should be feasible to extend to other transition metals or metal oxide systems, which will be the part of ongoing work.

Acknowledgement

The authors also extend their sincere appreciation to the Deanship of Scientific Research at King Saud University for funding the work through the Research Group No. RG-1437-004.

References

1. X. Xia, Y. Zhang, D. Chao, C. Guan, Y. Zhang, L. Li, X. Ge, I. M´ınguez Bacho, J. Tu and H. J. Fan, Nanoscale, 2014, **6**, 5008
2. C. Largeot, C. Portet, J. Chmiola, P. Taberna, Y. Gogotsi and P. Simon, J. Am. Chem. Soc., 2008, **130**, 2730.
3. G. Wang, L. Zhang and J. Zhang, Chem. Soc. Rev., 2012, **41**, 797.
4. P. Simon and Y. Gogotsi, Nat. Mater., 2008, **7**, 845.
5. Y. R. Ahn, M. Y. Song, S. M. Jo and C. R. Park, Nanotechnol., 2006, **17**, 2865.
6. C. C. Hu, Y. H. Huang and K. H. Chang, J. Power Sources, 2002, **108**, 117.
7. J. Jiang and A. Kucernak, Electrochim. Acta, 2002, **27**, 2381.
8. S. Vijayakumar, S. Nagamuthu, and G. Muralidharan, ACS Appl. Mater. Interfaces, 2013, **5**, 2188.
9. M. M. Liu, J. Chang, J. Sun and L. Gao, RSC Adv., 2013, **3**, 8003.
10. S. W. Bian and L. Zhu, RSC Adv., 2013, **3**, 4212.
11. N. Miura, S. Oonishi and K. Rajendra, Electrochem. Solid-State Lett., 2004, **7**, 247.
12. S. Chaudhari, D. Bhattacharjya and J. S Yu, RSC Adv., 2013, **3**, 25120
13. C. C. Hu, C. M. Huang and K. H. Chang, J. Power Sources, 2008, **185**, 1594.
14. C. Yuan, X. Zhang, L. Su, B. Gao and L. Shen, J. Mater. Chem., 2009, **19**, 5772
15. R. R. Bi, X. L. Wu, F. F. Gao, L. Y. Jiang, Y. G. Guo and L. J. Wan, J Phys. Chem. C, 2010, **114**, 2448
16. P. V. Kamath, G. Helen, A. Therese and J. Gopalakrishnan, J. Solid State Chem., 1997, **128**, 38.
17. M. S. Wu, Y. A. Huang, C. H. Yang and J. J. Jow, Int. J. of Hydro. Energy, 2007, **32**, 4153.
18. J. W. Lee, J. M. Ko and J. D. Kim, J. Phys. Chem. C, 2011, **115**, 19445.
19. D. P. Dubal, V. J. Fulari and C. D. Lokhande, Microporous Mesoporous Mater., 2012, **151**, 511.
20. S. K. Meher, P. Justin and G. Ranga Rao, Nanoscale, 2011, **3**, 683.
21. A. D. Jagadale, V. S. Kumbhar, D. S. Dhawale and C. D. Lokhande, Journal of Electroanal. Chem., 2013, **704**, 90.
22. B. Sarma, R. S. Ray, S. K. Mohanty and M. Misra, Appl. Sur. Sci., 2014, **300**, 29.
23. B. K. Sharma, Electrochemistry, Goel publishing house, Fifth edition, 1997, 153-169.
24. J. J. Feng, A. Q. Li, A. J. Wang, Z. Lei and J. R. Chen, Microchim Acta, 2011, **173**, 383.
25. Y. Chen, Y. Wang, P. Sun, P. Yang, L. Du and W. Mai, J. Mater. Chem. A, 2015, **3**, 20614.
26. R. S. Mane, Y. H. Hwang, C. D. Lokhande, S. D. Sartale and S. H. Han, Appl. Surf. Sci., 2005, **246**, 271.
27. M. M. Vadiyar, S. C. Bhise, S. K. Patil, S. S. Kolekar, A. R. Shelke, N. G. Deshpande, J.-Y. Chang, K. S. Ghule, A. V. Ghule, Chem. Comm., 2016, 52, 2557.
28. J. W. Lang, L. B. Kong, W. J. Wu, Y. C. Luo and L. Kang, Chem. Comm., 2008, 4213.
29. B. E. Conway, J. Electrochem. Soc., 1991, **138**, 1539.
30. S. K. Meher, P. Justin and G. R. Rao, Electrochim. Acta, 2010, **55**, 8388.
31. R. B. Rakhi, W. Chen, D. Cha and H. N. Alshareef, Nano. Lett., 2012, **12**, 2559.
32. V. Srinivasan and J. W. Weidner, J. Electrochem. Soc., 2000, **147**, 880.
33. W. Sugimoto, H. Iwata, Y. Yasunaga, Y. Murakami and Y. Takasu, Angew. Chem, Int. Ed. 2003, **42**, 4092.
34. T. L. Kelly, K. Yano and M. O. Wolf, ACS Appl. Mater. Interfaces 2009, **1**, 2536.
35. B. Saravanakumar, K. K. Purushothaman and G. Muralidharan, ACS Appl. Mater. Interfaces, 2012, **4**, 4484.
36. J. Li, W. Zhao, F. Huang, A. Manivannan and N. Wu, Nanoscale, 2011, **3**, 5103.
37. C. Yuan, X. Zhang, L. Su, B. Gao and L. Shen, J. Mater. Chem., 2009, **19**, 5772.
38. Z. B. Wen, Q. T. Qu, Q. Gao, X. W. Zheng, Z. H. Hu, Y. P. Wu, Y. F. Liu and X. J. Wang, Electrochem. Comm., 2009, **11**, 715.
39. A. G. Pandolfo and A. F. Hollenkamp, J. Power Sources, 2006, **157**, 11.
40. A. A. Radhiyah, M. I. Izwan, V. Baiju, C. K. Feng, I. Jamil and R. Jose, RSC Adv., 2015, **13**, 9667.
41. Y. Li, K. Huang, Z. Yao. S. Liu and X. Qing, Electrochimica Acta, 2011, **56**, 2140.

Nanomorphology-dependent pseudocapacitive properties of NiO electrodes engineered through controlled potentiodynamic electrodeposition process

Rohan M. Kore, Rajaram S. Mane, Mu. Naushad, Mohammad R. Khan and Balkrishna J. Lokhande

Graphical Abstract-